Journal of Environmental Chemical Engineering 12 (2024) 112426

Contents lists available at ScienceDirect

Journal of Environmental Chemical Engineering

journal homepage: www.elsevier.com/locate/jece

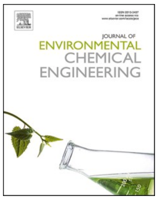

Conversion of CoNiFe-LDH to CoNiFe-MOF/LDH as catalyst for efficient heterogeneous electro-Fenton degradation of sulfonamide antibiotics

Bing-Qing Wu [a,1], Shu-Ting Cheng [a,1], Xiao-Fang Shen [a,b], Yue-Hong Pang [a,b,*]

[a] *State Key Laboratory of Food Science and Resources, School of Food Science and Technology, Collaborative Innovation Center of Food Safety and Quality Control in Jiangsu Province, Jiangnan University, Wuxi 214122, China*
[b] *International Joint Laboratory on Food Safety, Jiangnan University, Wuxi 214122, China*

ARTICLE INFO

Editor: Wesaal Khan

Keywords:
Layered double hydroxide
Metal-organic frameworks
Heterogeneous electro-Fenton
Sulfonamides
Water treatment

ABSTRACT

The widespread use of antibiotics leads to spread of resistance bacteria and genes in natural water and has a potential threat to human health. Herein, a nanorod CoNiFe-MOF/LDH was synthesized using a self-sacrificial strategy and employed to degrade sulfamethazine (SMT) by heterogeneous electro-Fenton (HEF). The conversion of CoNiFe-LDH to CoNiFe-MOF/LDH resulted in a significant enhancement of specific surface area (from 13.96 to 32.26 $m^2\ g^{-1}$) and electroactive surface area (from 2.20 to 4.22 mm^2), and the degradation rate of SMT increased from 88.53% to 98.41% within 60 min. The free radical capture experiments indicated that ·OH and $^1O_2$ played a significant role in the HEF process. The CoNiFe-MOF/LDH catalyst could be recycled 5 times with degradation rate of over 90%, it also demonstrated excellent resistance towards inorganic ions and humic acid. In addition, the CoNiFe-MOF/LDH exhibited remarkable degradation efficiency for 8 sulfonamides (over 89%). Mass spectrometry analysis indicated that SMT was oxidatively degraded via three possible pathways. According to the analysis of Toxicity Estimation Software Tool, the acute toxicity of SMT was effectively weakened. The CoNiFe-MOF/LDH catalyst has potential application prospect in wastewater treatment.

1. Introduction

Antibiotics have been used extensively around the world, causing their release and accumulation at least ng/L in natural water including lakes, rivers, and even drinking water [1]. Due to antibiotics are incompletely absorbed in organisms, about 80% of ingested antibiotics are discharged into the environment [2]. The majority of these residual antibiotics are released into surface water, soil, and groundwater [3]. Their antibacterial activity can be maintained from a few days to more than a year hinging on their chemical structure, initial concentrations, half-life and environmental conditions [4]. Antibiotics may induce chronic effects on aquatic organisms at prolonged exposure, such as changes in behavior, growth and reproduction [5], its residues in the environment expedited the development of antibiotic-resistant bacteria or genes [6]. Hence, it is of great significance to develop efficient methods to degrade antibiotics in wastewater.

Various techniques utilized for degradation of antibiotics from wastewater include biodegradation, adsorption , membrane filtration and coagulation-flocculation [7]. However, the oxidative capabilities of biological treatment are insufficient for degradation of the majority of pharmaceuticals and their metabolites, other physical and physico-chemical methods simply transfer these substances from one phase to another or generate concentrates, failing to solve destruction of antibiotics [8]. Advanced oxidation processes (AOPs) are an effective method to eliminate toxic and persistent organic pollutants [9]. The electro-Fenton (EF), a type of AOPs has received extensive attention due to its high efficiency and easy automatic control [10]. However, the practical applicability of EF is limited by the high concentration of ionic iron and the difficulty of recyclability [11].

To overcome the limitation, the heterogeneous EF (HEF) using solid catalysts in solution has been largely developed showing its biodegradable products, less secondary pollution as well as good recyclability compare with homogeneous EF process [12,13]. Due to the majority of Fe-containing catalysts tend to agglomerate, they are prone to active site loss and the release of excessive Fe^{3+}/Fe^{2+} ions over time, ultimately leading to a decrease in pollutant removal efficiency within the system

---

[*] Corresponding author at: State Key Laboratory of Food Science and Resources, School of Food Science and Technology, Collaborative Innovation Center of Food Safety and Quality Control in Jiangsu Province, Jiangnan University, Wuxi 214122, China.

E-mail address: yhpang@jiangnan.edu.cn (Y.-H. Pang).

[1] Co-first Author: These authors contribute equally.

https://doi.org/10.1016/j.jece.2024.112426
Received 25 December 2023; Received in revised form 28 February 2024; Accepted 6 March 2024

[14]. Moreover, the complex preparation methods of heterogeneous catalysts are difficult to be applied in large-scale practical applications [15]. Therefore, there is a critical need to develop efficient and durable heterogeneous Fenton catalysts with a facile preparation strategy for degradation of antibiotics.

Layered double hydroxides (LDHs), a two-dimensional layered anionic clay material [16,17], have been applied in wastewater treatment for their unique layered structure and intrinsic catalytic activity [18,19]. The electrocatalytic performance of LDHs is restricted by small specific surface area, low conductivity, and easy aggregation [20]. The current research focuses on improving the performance of LDHs by incorporating with materials of good conductivity into LDHs, such as various metals, carbon nanomaterials and magnetic materials [21]. MOFs have emerged as a versatile platform for fabrication of novel electrocatalysts owing to large surface areas, adjustable coordination environments, and excellent conductivity [22,23]. The conversion of LDHs to MOFs can combine flexible structure and conductivity of MOF and variety and intrinsic catalytic performance of LDH [24]. Therefore, our motivation was to convert LDH into MOF, expecting that the conversion would provide a larger specific surface area and excellent electrical conductivity for capturing and transferring electrons, and improve the catalytic performance and degradation efficiency of MOF/LDH.

Herein, the trimetallic CoNiFe-LDH as a template was converted to heterostructured CoNiFe-MOF/LDH by a hydrothermal reaction. Sulfamethazine (SMT), a sulfonamides antibiotic widely used to treat infectious animals and humans, was chosen as a model. CoNiFe-MOF/LDH was used as catalyst to degrade SMT by the HEF. The critical factors influencing degradation of SMT were examined in detail, including initial pH, applied current, catalyst dosage and so on. The degradation efficiency of common sulfonamide antibiotics and the catalyst stability in HEF were investigated. The main free radicals and degradation pathways were elucidated according to radical capture experiments and mass spectrometry (MS). The toxicity of SMT and its intermediates was assessed by the Toxicity Estimation Software Tool (T.E.S.T.).

2. Experimental methods

2.1. Reagents and chemicals

The reagents and chemicals were provided in Text S1 of the supporting information.

2.2. Synthesis of CoNiFe-MOF/LDH catalyst

The synthesis of CoNiFe-MOF/LDH catalyst was schematized in Fig. 1. The CoNiFe-LDH was synthesized according to previous literature [24] with minor modifications.

The CoNiFe-LDH was synthesized following a solvothermal method. $CoCl_2 \cdot 6H_2O$ (1.20 mM), $NiCl_2 \cdot 6H_2O$ (0.25 mM), $FeCl_2 \cdot 4H_2O$ (0.15 mM), and urea (6.3 mM) were mixed in 10 mL Milli-Q water. The obtained solution was transferred into Teflon-lined stainless autoclave for hydrothermal treatment at 120°C for 12 h. Afterwards, the obtained CoNiFe-LDH templates were dried at 90°C for 12 h after washing with water and anhydrous ethanol several times.

Then, the obtained CoNiFe-LDH template was dispersed in a 20 mL N,N-dimethylformamide (DMF) solution containing an excess of 2,3,6,7,10,11-Hexahydroxytriphenylene hydrate (HHTP). This mixed solution was heated at 100°C for 24 h. After the reaction, the black product was washed with water, DMF, and ethanol through centrifugation, subsequently dried in a vacuum at 90°C overnight to obtain CoNiFe-MOF/LDH. The CoNi-MOF/LDH was synthesized by a similar process, except that no $FeCl_2 \cdot 4H_2O$ was added to the precursor.

2.3. HEF degradation process

In the HEF process, the antibiotics were degraded in a reactor containing 150 mL of 0.05 mol/L Na_2SO_4. The cathode and anode were parallelly fixed with a 2 cm distance in the reactor. The Pt electrode (1 cm × 2 cm) was used as an anode and purchased from Wuhu Kezhao New Materials Co. Ltd. (Anhui, China). The hydrophobic microporous laminated carbon paper (HML-CP) (2 cm × 2.5 cm) was chosen as a cathode and fabricated by Wuhu Eryi Material Technology Co. (Anhui, China). Oxygen generator was provided by Jiangsu Yuyue Co. Ltd. (Jiangsu, China) to supply O_2 (95%) with the 0.8 L /min of flow rate. The HEF treatments used a DC power source (HY3005ET, China) to supply current.

2.4. Characterization methods

The morphologies of the obtained catalysts were observed by field emission scanning electron microscopy (SEM, Hitach, Japan) and transmission electron microscopy (TEM, FEI Tecnai F20, America). X-ray diffraction (XRD) patterns were analyzed by a diffractometer (XRD, D2 PHASER, Germany). The catalysts were characterized by fourier-transformed infrared spectroscopy (FT-IR, Nicolet IS10, America). The specific surface areas and the pore size distributions of the catalysts were calculated using the Brunauer-Emmett-Teller (BET) theory (BET, Micromeritics ASAP 2460, America). The element-binding environments were analyzed with X-ray photoelectron spectroscopy (XPS, Thermo Scientific K-Alpha, America). Total organic carbon (TOC) was measured by using a TOC analyzer (TOC, Jena Multi N/C 3100, Germany). More details of the analytical methods and electrochemical

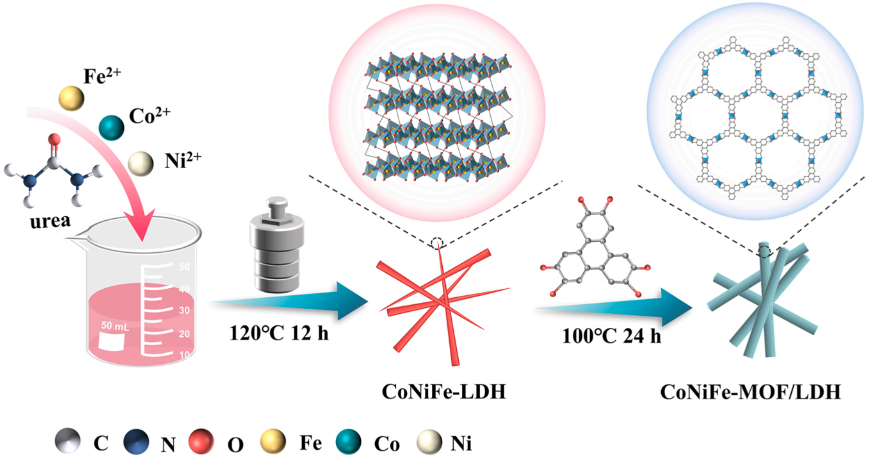

Fig. 1. Illustration of synthesis route of the CoNiFe-MOF/LDH catalyst.

measurements were presented in the Text S2–3 of supporting information.

3. Results and discussions

3.1. Characterization of the catalysts

The morphology of CoNiFe-MOF/LDH composite and CoNiFe-LDH

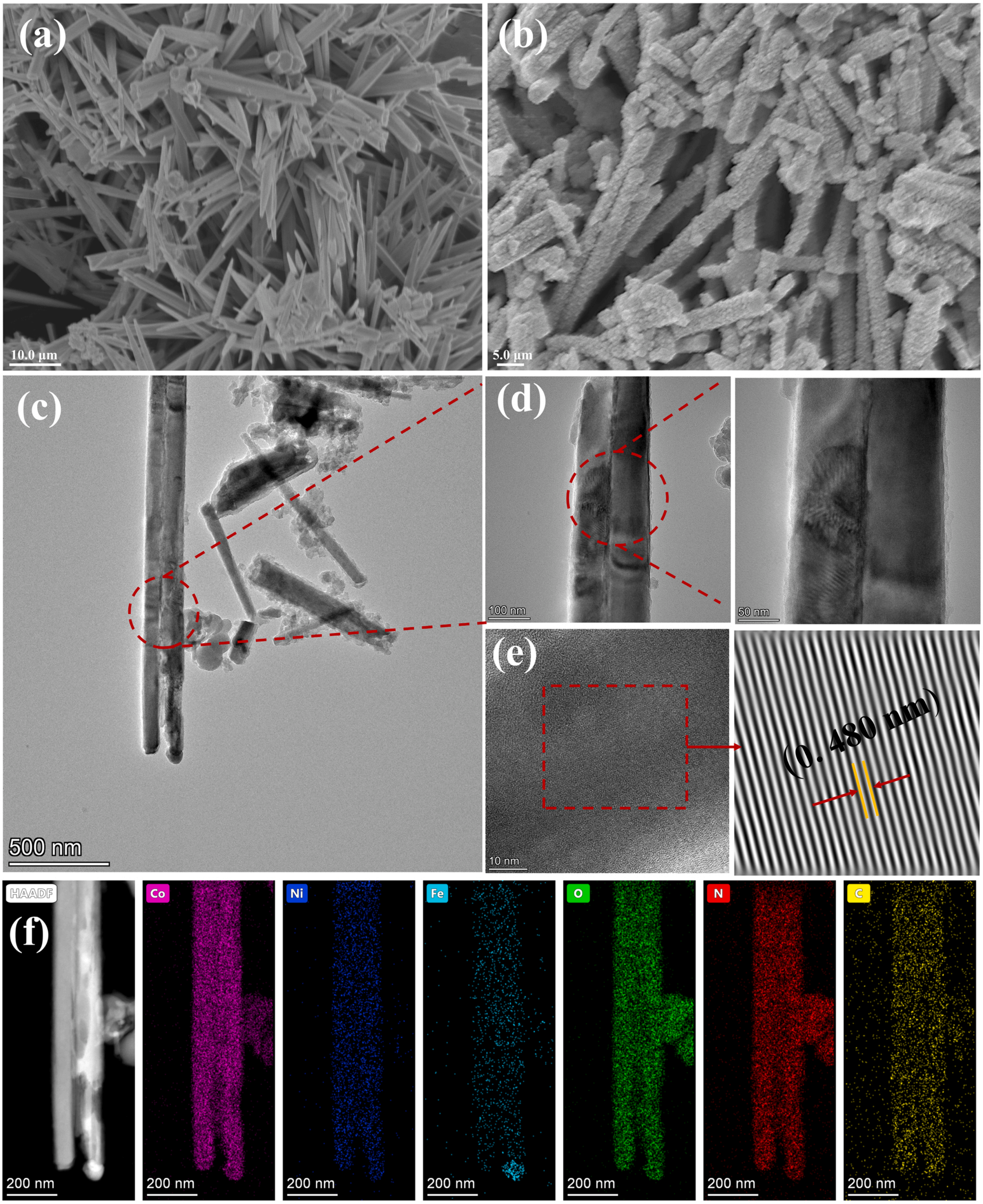

Fig. 2. (a) SEM image of CoNiFe-LDH; (b) SEM image of CoNiFe-MOF/LDH; (c-d) TEM image of CoNiFe-MOF/LDH; (e) High-resolution TEM of CoNiFe-MOF/LDH; (f) Elemental mapping of CoNiFe-MOF/LDH.

template were observed by SEM and TEM. The CoNiFe-LDH showed an agglomerated morphology with regular and smooth nanowires (Fig. 2a). The CoNiFe-LDH was employed as a template for integrating organic ligands (HHTP), resulting in the transformation of the threadlike morphology to the claviform CoNiFe-MOF/LDH (Fig. 2b). The as-synthesized products featured compact and rough rods with an average diameter of 70–208 nm (Fig. 2c-d). Fig. 2e showed the high-resolution TEM images of CoNiFe-MOF/LDH with lattice distances of 0.48 nm, which was ascribed to the (020) crystal planes. From the elemental mapping images (Fig. 2f), the C, N, O, Co, Ni, and Fe elements exhibited a uniform distribution of CoNiFe-MOF/LDH, indicating that CoNiFe-MOF/LDH could provide abundant active sites for H_2O_2 activation [25].

The crystal structure of the synthetic catalysts was analyzed by XRD (Fig. 3a). The diffraction peaks of CoNiFe-MOF/LDH at 9.97°, 17.19°, and 19.97° corresponded to the (100), (110), and (021) crystal planes of $Co(OH)(CO_3)_{0.5}\cdot 0.11\ H_2O$ (JCPDS 48–0083), respectively. The diffraction peak of HHTP at 27.04° was also observed in the CoNiFe-MOF/LDH, showing the CoNiFe-LDH was combined with HHTP. Meanwhile, XRD patterns of CoNi-MOF/LDH and CoNiFe-MOF/LDH showed that the introduction of Fe unchanged in the original crystal structure.

The functional groups of CoNiFe-LDH, CoNiFe-MOF/LDH, and CoNi-MOF/LDH were analyzed by FT-IR (Fig. 3b). The absorption peaks at around 753, 1375 and 3514 cm^{-1}, were associated with the bending vibration of C-H, the stretching vibrations of C═O, and the O-H of interlayer water molecules, respectively [26,27]. A broad shoulder band between 1480 and 1517 cm^{-1} might be related to the change of free carbonates in symmetry [28]. It is worth noting that the peaks at 1258 cm^{-1} and 1654 cm^{-1} of CoNiFe-MOF/LDH and CoNi-MOF/LDH, were attributed to the C-O stretching vibration of backbone on the organic ligand, and the C-C stretching vibration of aromatic backbone chain, respectively [20,29]. This indicated the CoNiFe-LDH successfully

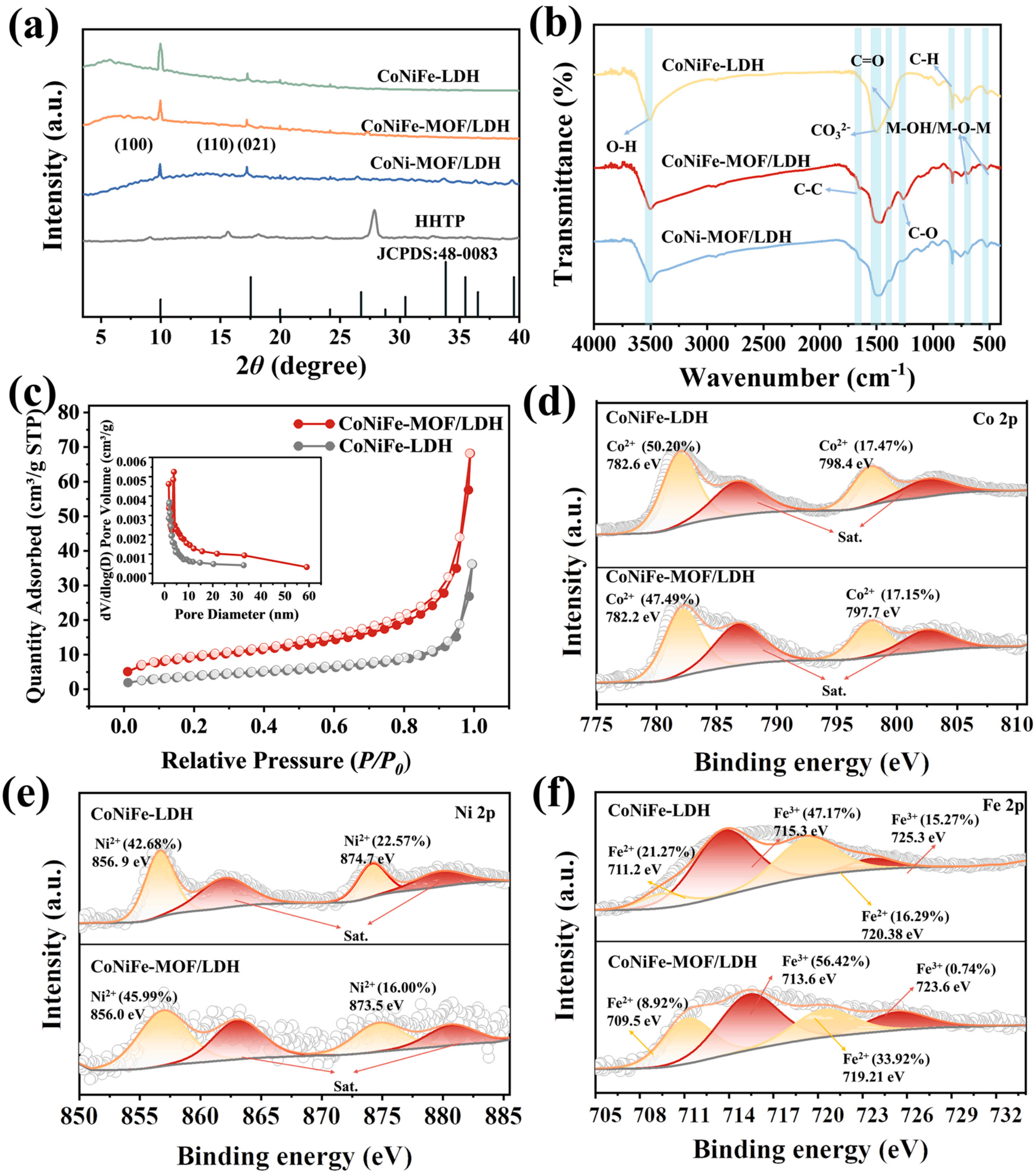

Fig. 3. (a) XRD patterns of synthetic catalysts; (b) FT-IR spectra of synthetic catalysts; (c) N_2 adsorption-desorption isotherm and the corresponding pore size distribution curve (insert) of synthetic catalysts; High-resolution XPS of (d) Co 2p; (e) Ni 2p and (f) Fe 2p for CoNiFe-MOF/LDH and CoNiFe-LDH.

converted to CoNiFe-MOF/LDH. In addition, the absorption peaks at around 691 cm^{-1} and 526 cm^{-1} of three catalysts, were ascribed to vibrations of the M-OH and M-O-M bonds [30]. These metal-oxygen bonds were instrumental in facilitating electron transfer among Fe, Ni, and Co, thereby enabling the activation of H_2O_2 [31].

The CoNiFe-LDH and CoNiFe-MOF/LDH showed different N_2 adsorption-desorption isotherms in Fig. 3c. The CoNiFe-LDH followed type II isotherms, indicating the physical adsorption mechanism observed in non-porous or microporous adsorbents. Whereas the CoNiFe-MOF/LDH conformed to the type IV isotherms with significant hysteresis back in the medium relative pressure range ($P/P_0 > 0.5$) of N_2 adsorption, indicating the presence of ordered mesopores [32]. Compared to CoNiFe-LDH, the specific surface area (from 13.96 to 32.26 $m^2\ g^{-1}$) and pore volume (from 0.024 to 0.054 $cm^3\ g^{-1}$) of CoNiFe-MOF/LDH (Table S1) were beneficial to enhancing the interaction between oxygen and organic molecules.

Chemical composition of the CoNiFe-LDH and CoNiFe-MOF/LDH was characterized by XPS. Fig. S1 showed that C, N, O, Co, Ni, and Fe elements co-existed in the CoNiFe-LDH and CoNiFe-MOF/LDH, and the atomic percentage of elements was summarized in Table S2. In addition, the C 1 s high-resolution spectrum of CoNiFe-LDH (Fig. S2) consisted of three component peaks at 284.8, 289.7, and 286.2 eV, corresponding to C-C, C═O, and C-O, respectively [33]. Compared to CoNiFe-LDH template, C atoms linked to O-containing groups showed a reduced peak intensity in the C 1 s spectrum of CoNiFe-MOF/LDH. This reduction was ascribed to the O-containing functional groups as anchors for the graft growth of CoNiFe-LDH nanowire, facilitating the conversion to MOF/LDH [28]. The O 1 s spectrum of CoNiFe-LDH was decomposed into two peaks at 533.8 and 532.1 eV, attributed to C-O and C═O respectively (Fig. S3) [34]. The conversion of MOF/LDH caused a prominent rise in the relative proportion of C-O (from 13.26% to 67.95%) in the CoNiFe-MOF/LDH, which was consistent with a higher number of electrons being transferred from oxygen to the metal centers [35].

As shown in Fig. 3d, peaks at 782.6 and 798.4 eV were attributed to Co^{2+} in the CoNiFe-LDH, the satellite peaks at 786.8 and 802.6 eV were also observed [36]. The Ni 2p spectrum of CoNiFe-LDH showed two characteristic peaks at 856.9 and 874.7 eV, corresponding to the valence states of Ni^{2+}. (Fig. 3e) [37]. As displayed in Fig. 3f, Fe^{2+} could be fitted to the Fe $2p_{3/2}$ and Fe $2p_{1/2}$ of CoNiFe-LDH, and attributed to 711.2 and 720.4 eV, respectively [38,39]. The peaks at 715.3 and 725.3 eV were corresponded to Fe^{3+} in the Fe $2p_{3/2}$ and Fe $2p_{1/2}$, respectively [40]. In addition, all characteristic peaks of the Co, Ni and Fe were also found in the CoNiFe-MOF/LDH composites (Fig. 3d-f). And after coordination with HHTP linkers, Co 2p, Ni 2p and Fe 2p peaks of CoNiFe-MOF/LDH shifted to lower binding energies of approximately 0.4, 0.9 and 1.7 eV respectively, which were helpful for enhancing electron-accepting features and electron transfer at the surface of catalysts [41].

3.2. *Electrochemical performance of the catalysts*

Electrochemical behaviors of CoNiFe-LDH and CoNiFe-MOF/LDH were analyzed by cyclic voltammetry (CV) and electrochemical surface area (ECSA). Fig. 4a showed CV curves of CoNiFe-LDH at various scanning rates, and anodic peak currents of catalyst exhibited a linear relationship with the square root of scanning rate (Fig. 4c). Similarly, the result of CoNiFe-MOF/LDH was also consistent with CoNiFe-LDH (Figs. 4b, 4d), which suggested the redox reaction of two catalysts was controlled by diffusion [42]. Based on the Randles-Sevcik equation, the ECSA of CoNiFe-LDH was calculated to be 2.20 mm^2. After converting to CoNiFe-MOF/LDH, the ECSA increased to 4.22 mm^2. The increase facilitated the exposure of additional electroactive sites, thereby promoting the generation and activation of H_2O_2 [43]. Compared with the CoNiFe-LDH, CV curves of CoNiFe-MOF/LDH (Fig. S4) showed an obvious redox peak enhancement between 0.15 ~ 0.25 V. The structure was favorable for fast charge migration, strong redox activity, and

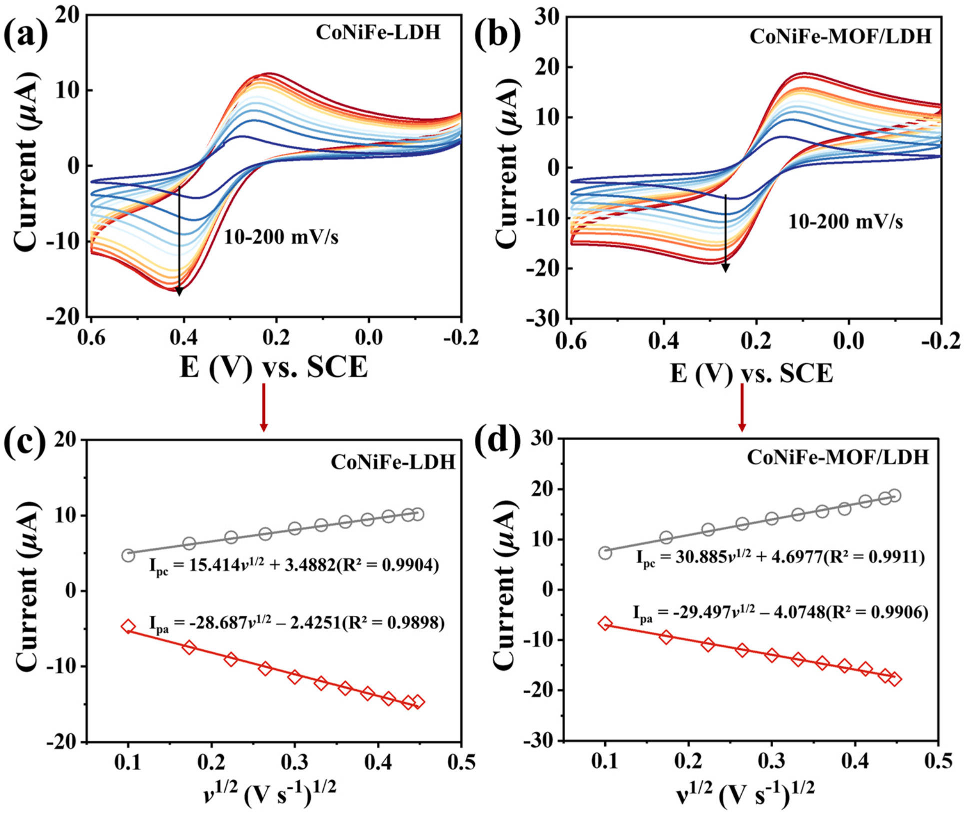

Fig. 4. CV curves of (a) CoNiFe-LDH and (b) CoNiFe-MOF/LDH at various scan rates. The linear relationship between the peak current of (c) CoNiFe-LDH, (d) CoNiFe-MOF/LDH and the square root of the scan rate.

excellent electrical conductivity [44].

3.3. SMT degradation performance by catalysts in the HEF

The performance of different catalysts was investigated in SMT degradation by electrochemical oxidation (EO), adsorption, and HEF process (Fig. 5a). The SMT adsorption of CoNiFe-MOF/LDH within 60 min showed a removing rate of 14.76%, EO occurred on the electrode was 32.86%. The degradation rate was 48.67% and 88.53% by CoNi-LDH, CoNiFe-LDH in the HEF process, respectively, which indicated the introduction of third metal (Fe) into the layers of LDH could improve catalytic performance by shortening the electron transfer distance and exposing active sites [45]. After conversion of LDH to MOF/LDH, the degradation rate increased to 82.89% and 98.41% by CoNi-MOF/LDH and CoNiFe-MOF/LDH, respectively, indicating excellent catalytic performance of CoNiFe-MOF/LDH in degradation process.

Kinetics of degradation rate were investigated during the HEF process by zero-order, first-order, and second-order models (Table S3). First-order model showed the highest correlation coefficient (R^2) for CoNiFe-LDH and CoNiFe-MOF/LDH and the k value of CoNiFe-MOF/LDH (0.0663 min^{-1}) was higher than CoNiFe-LDH (0.0363 min^{-1}) and CoNi-MOF/LDH (0.0277 min^{-1}), respectively.

The performance of EF reactions is significantly affected by the applied current, catalyst dosage, initial pH, and initial SMT concentration. Consequently, the effect of these primary parameters was investigated for degradation SMT in the HEF process (Fig. 5b-e). The effects of applied current on SMT degradation and the kinetics of degradation rate were shown in Fig. 5b, S6. The degradation rate of SMT was 93.57%, 95.86%, 98.41%, and 96.55% at applied current of 5.0, 15.0, 25.0, and 35.0 mA, respectively (Fig. 5b) and k values were 0.0438, 0.0513, 0.0663, 0.0476 min^{-1} (Fig. S6), respectively. The degradation rate was decreased at currents of 35.0 mA, which was due to the occurrence of side reactions at a high current, such as the 4e-ORR pathway and the hydrogenolysis reaction (Eqs. (1) and (2)). The reaction of excess H_2O_2 with hydroxyl radicals (·OH) (Eq. (3)) could lead to decrease degradation rate [46].

$$O_2 + 4H^+ + 4e^- \rightarrow 2H_2O \qquad (1)$$

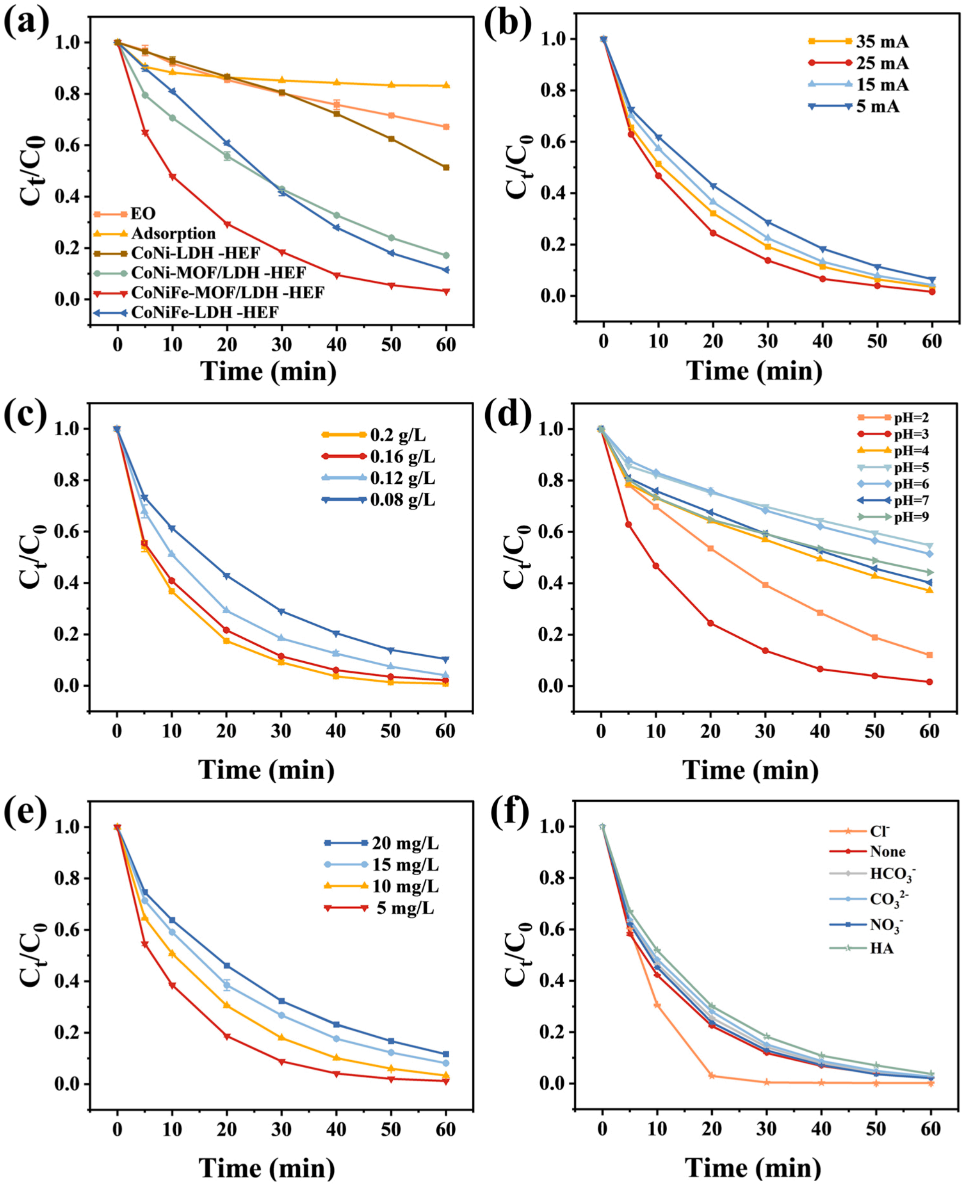

Fig. 5. (a) The SMT degradation performance in various reactions; Effects of (b) current; (c) catalyst dosage; (d) initial pH; (e) initial SMT concentration and (f) various anions and humic acid on the SMT degradation in the HEF system.

$$2H^{+} + 2e^{-} \rightarrow H_2 \quad (2)$$

$$\cdot OH + H_2O_2 \rightarrow H_2O + HO_2^{\cdot} \quad (3)$$

Catalysts can provide more active sites for generating reactive oxygen species (ROS); therefore, catalyst dosage is an important factor in HEF process. The CoNiFe-MOF/LDH dosage increased from 0.08 g/L to 0.16 g/L, the degradation rates of SMT increased from 89.61% to 97.92% (Fig. 5c) and the k values increased from 0.0372 to 0.0631 min^{-1} (Fig. S7). The catalyst dosage was further increased to 0.2 g/L, and the k-value was increased to 0.0802 min^{-1}, while the degradation rate only increased by 1.28%. This limitation may be related to H_2O_2 concentration and mass transfer efficiency between the catalyst and SMT. In addition, the excess catalyst could agglomerate causing the reduction of surface-active sites [47].

The reactivity of metal-containing catalyst is influenced by the pH level of solution. The pH range (pH 2–9) of solution was investigated by HEF reaction (Fig. 5d, S8). The best degradation rate was 98.41% at pH 3, which was due to the decline in oxidation potential of ·OH with increasement of pH (pH 0: $E^0 = +2.8$ V, pH 14: $E^0 = +1.98$ V) [48]. The degradation rate was 87.97% at pH 2 and the k value was 0.0336 min^{-1}. This decrease may be due to the high concentration of H^+ could compete with H_2O_2 and hinder the accumulation of ·OH [47]. However, the degradation effects of SMT were between 40% and 60% at pH 4–9, and k values were between 0.0090 min^{-1} and 0.0149 min^{-1}, which was that the oxidizing ability of ·OH was weakened at higher pH values, and the side reaction of H_2O_2 to form H_2O was increased [49].

The degradation efficiency of pollutants is also related to their initial concentrations (Fig. 5e, S9). The degradation rate was still 88.37% at initial SMT concentration of 20.0 mg/L, and the k value was 0.0347 min^{-1}, indicating that the HEF process had excellent degradation capability. The degradation rate slowed down with increasing initial SMT concentration. Although increasing the initial SMT concentrations can improve the mass transfer efficiency, the intermediates were also generated and competed with SMT for the reaction with ROS [47]. In addition, the mineralization rate was one of the key indicators of antibiotic degradation. The TOC rate of SMT was increased with duration of treatment time and reached 85.66% at 420 min in the HEF process (Fig. S10), indicating the HEF process had a high level of mineralization.

Humic acid (HA) and inorganic anions such as NO_3^-, CO_3^{2-}, Cl^-, HCO_3^-, existed in the actual wastewater and could influence the degradation of antibiotics (Fig. 5f). Among them, only Cl^- acted as a promoter of SMT degradation and the degradation rate reached 99.59% within 30 min. Due to Cl^- supplied electrons to generate Cl· ($E_0 = 2.4$ $_{VNHE}$) and $ClOH\cdot^-$ ($E_0 = 1.5 \sim 1.8$ $_{VNHE}$), and subsequently formed $Cl_2\cdot^-$ ($E_0 = 2.0$ $_{VNHE}$) (Eqs. (4) and (5)). $Cl_2\cdot^-$ can degrade SMT through H-abstraction and single-electron oxidation [50]. Presence of other anions (NO_3^-, CO_3^{2-}, HCO_3^-) and HA resulted in a degradation rate of about 96%, indicating that these anions and HA could partially consume ·OH (Eqs. (6)–(8)).

$$Cl^- + \cdot OH \rightarrow ClOH\cdot^- \quad (4)$$

$$Cl^- + ClOH\cdot^- \rightarrow Cl_2\cdot^- + OH^- \quad (5)$$

$$NO_3^- + \cdot OH \rightarrow OH^- + \cdot NO_2 \quad (6)$$

$$CO_3^{2-} + \cdot OH \rightarrow OH^- + CO_3\cdot^- \quad (7)$$

$$HCO_3^- + \cdot OH \rightarrow H_2O + CO_3\cdot^- \quad (8)$$

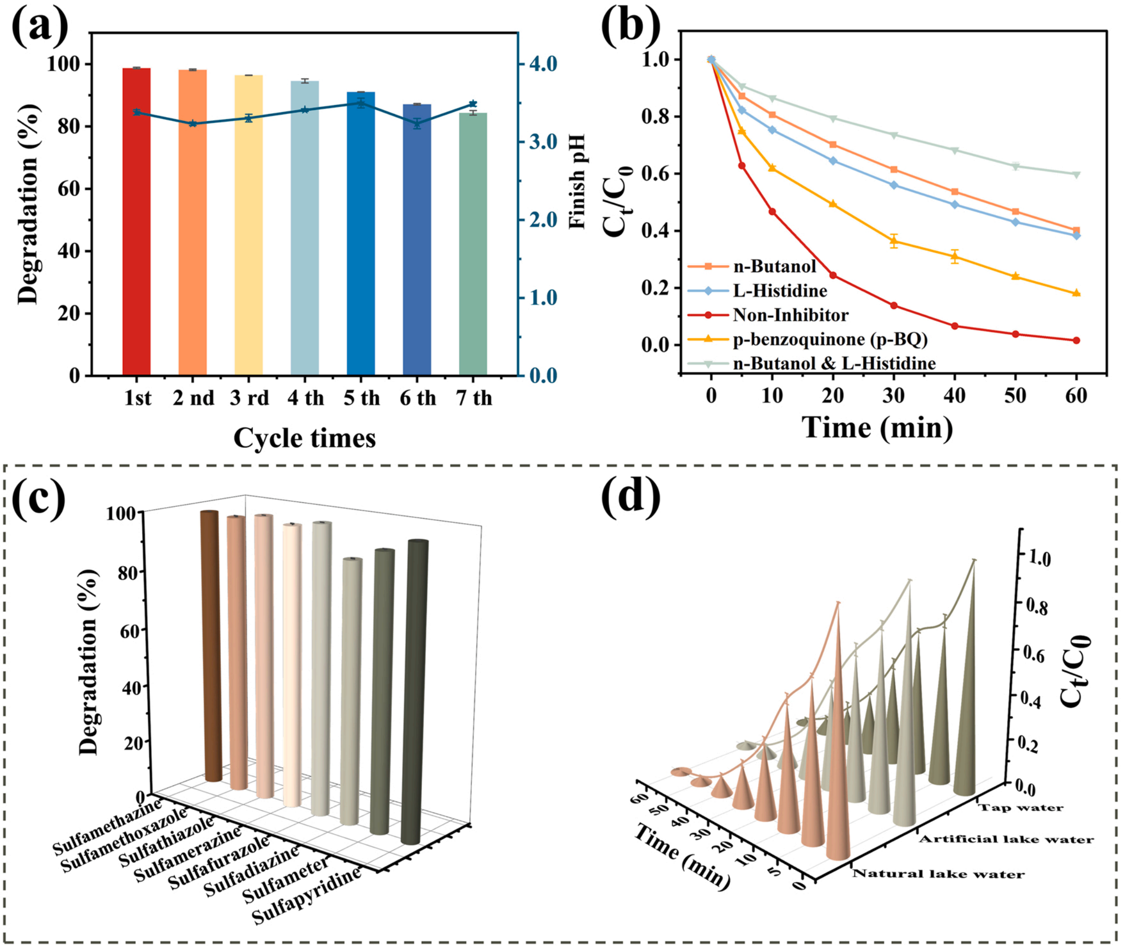

Fig. 6. (a) Influences of reused catalyst on SMT degradation; (d) Effect of different capture agents on SMT degradation; (c) Degradation rates of several sulfonamide antibiotics; (d) The degradation rates of SMT in different water samples.

3.4. Application of the CoNiFe-MOF/LDH catalyst and mechanism analysis

To enable sustainable application in practical wastewater treatment, reusability of catalyst was studied in Fig. 6a. The degradation rates started to decrease in the third cycle (96.39%), and the degradation rate was still above 90% after five cycles. The obvious deceleration was attributed to surface passivation and deactivation, leading to spontaneous acidification. The pH values before and after the reaction increased from pH 3 to about pH 3.5, which was attributed to the precipitation of H_2 after the hydrogen hydrolysis reaction [51].

At the same time, $\cdot OH$, $\cdot O_2^-$ and $^1O_2$ radical capture tests were conducted to investigate their contribution in the HEF process (Fig. 6b). In particular, $\cdot OH$ has very short lifetimes of 10^{-9} to 10^{-7} s compared with other radicals [52]. The 300 mM n-butanol was introduced into the solution, and the degradation rate of SMT decreased to 59.83% (reduced by 38.58%), addition of 10 mM p-benzoquinone (p-BQ) resulted in degradation rate of 82.07% (reduced by 16.34%), indicating that $\cdot OH$ and $\cdot O_2^-$ had different degree in inhibition of the HEF. The L-histidine (10 mM), as $^1O_2$ scavenger, was introduced into the SMT solution, the degradation decreased from 98.41% to 61.71%, reducing by 36.70%. This decrease indicated that $^1O_2$ also accounted for major portion of the SMT degradation. In addition, the degradation rate of SMT significantly reduced from 98.41% to 40.15% when L-histidine and n-butanol were simultaneously introduced into the solution, indicating that $\cdot OH$ and $^1O_2$ played a crucial role in the HEF process.

CoNiFe-MOF/LDH as catalyst in the HEF process for degrading other sulfonamide antibiotics was investigated in Fig. 6c. Sulfathiazole and sulfafurazole were completely degraded, whereas sulfamethoxazole (97.19%), sulfamerazine (96.92%), sulfadiazine (89.27%), sulfapyridine (98.00%) and sulfamater (93.95%) were efficiently degraded by the HEF process. Therefore, the CoNiFe-MOF/LDH in the HEF showed good universal applicability for degradation of sulfonamide antibiotics. The application of CoNiFe-MOF/LDH was further studied in real water samples (Fig. 6d). The degradation rates of SMT were 98.98%, 97.83%, 97.69% in natural lake water (Taihu lake, China Wuxi), tap water and artificial lake water, respectively. In addition, compared with recently reported Fenton catalysts for pollutant degradation (Table S4), this work demonstrated excellent degradation efficiency, high mineralizing capacity, low current and simple preparation method.

In addition, XPS of the fresh and used CoNiFe-MOF/LDH almost unchanged in the elemental composition (Fig. S11). The Co 2p, Fe 2p, Ni 2p spectra and intensity of the characteristic peaks of used CoNiFe-MOF/LDH was almost consistent with fresh catalysts (Fig. 7a-c). A remarkable change in the metal atomic percentage of fresh and used CoNiFe-MOF/LDH indicated that metals participated in Fenton reactions and low-valence metal ions and high-valence one can be interconverted. In Fig. 7d, the XRD patterns of corresponding fresh and used CoNiFe-MOF/LDH showed the crystallinity remained almost unaltered.

Based on the above analysis, Fig. 8 illustrated the possible mechanisms of ROS generation and antibiotics degradation on CoNiFe-MOF/

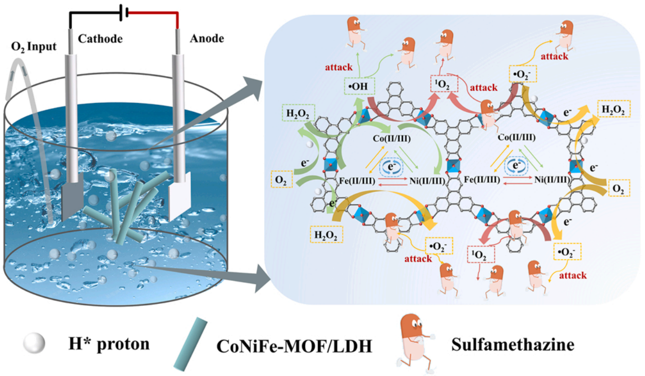

Fig. 8. Schematic diagram of the HEF system and involved chemical reactions.

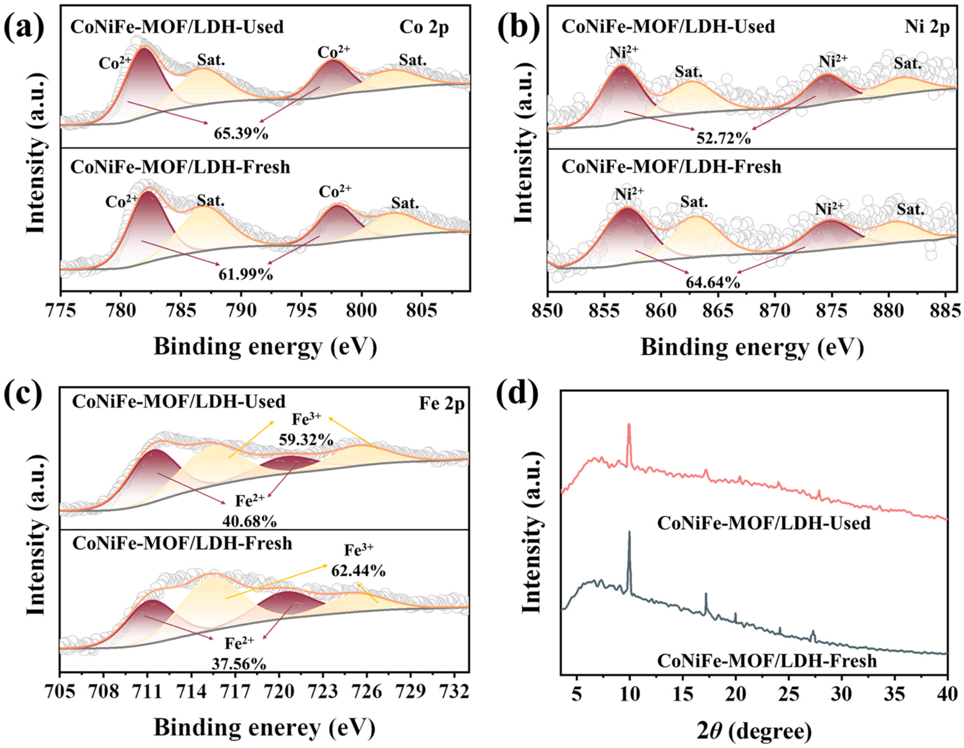

Fig. 7. The XPS spectra of fresh and used CoNiFe-MOF/LDH (a) Co 2p; (b) Ni 2p and (c) Fe 2p; (d) XRD patterns of CoNiFe-MOF/LDH were fresh and used in the degradation experiment.

LDH catalyst. The generation of ·OH was assigned to two pathways. Path 1: metal on the surface of CoNiFe-MOF/LDH activated H_2O_2, whereas Fe^{2+} / Co^{2+} / Ni^{2+} was oxidized to Fe^{3+} / Co^{3+} / Ni^{3+} simultaneously (Eq. (9)). Path 2: the anodic oxidation of water on the anode (Eq. (10)). The obtained trivalent transition-metal ions (Co^{3+} / Ni^{3+}) were reduced to divalent metal ions (Co^{2+} / Ni^{2+}) and the divalent metal ions (Fe^{2+} / Co^{2+}) were also oxidized to trivalent metal ions (Fe^{3+} / Co^{3+}) during EF reactions (Eqs. (11–12)), thereby the bivalent transition metal ions continuously activated H_2O_2 to generate ·OH [42,53]. The generation of $\cdot O_2^-$ was attributed to gain electrons on the cathode (Eqs. (13–14)), and the reaction of between H_2O_2 with Fe^{3+} / Co^{3+} / Ni^{3+} (Eq. (15)) [54]. $^1O_2$ has a longer lifetime (2–3.5 μs) in solution compared to ·OH [55], the generated $\cdot O_2^-$ further reacted with ·OH to produce $^1O_2$ (Eq. (16)) [43].

$$Fe^{2+} / Co^{2+} / Ni^{2+} + H_2O_2 \rightarrow Fe^{3+} / Co^{3+} / Ni^{3+} + \cdot OH + OH^- \tag{9}$$

$$H_2O - e^- \rightarrow \cdot OH + H^+ \tag{10}$$

$$Fe^{2+} + Co^{3+} / Ni^{3+} \rightarrow Fe^{3+} + Co^{2+} / Ni^{2+} \tag{11}$$

$$Co^{2+} + Ni^{3+} \rightarrow Ni^{2+} + Co^{3+} \tag{12}$$

$$O_2 + e^- \rightarrow \cdot O_2^- \tag{13}$$

$$\cdot O_2^- + 2H^+ + e^- \rightarrow H_2O_2 \tag{14}$$

$$Fe^{3+} / Co^{3+} / Ni^{3+} + H_2O_2 \rightarrow Fe^{2+} / Co^{2+} / Ni^{2+} + \cdot O_2^- + 2H^+ \tag{15}$$

$$\cdot O_2^- + \cdot OH \rightarrow {}^1O_2 + OH^- \tag{16}$$

3.5. Degradation pathway and toxicity analysis

The degradation products and possible pathways of SMT were investigated by MS. According to mass/charge ratios (*m/z*) (Table S5), three possible degradation pathways were proposed (Fig. 9). In pathway 1, SMT rearranged and formed P1 (*m/z* = 215). SMT and aniline portion of P1 were attacked by ·OH and $^1O_2$ to generate P2 (*m/z* = 229) and P3 (*m/z* = 245). In pathway 2, S-N bond of SMT was broken and generated P4 (*m/z* = 124) and P5 (*m/z* = 172). In pathway 3, C-N bond of SMT was cleaved to produce P6 (*m/z* = 205) acetimidamide compound with methane (1:1) [25]. Then the C-N bond of P6 was also broken to generate P7 (*m/z* = 186), which was oxidized and deaminated to form P8 (*m/z* = 165) [56,57]. Eventually, these products were finally mineralized to CO_2 and H_2O.

To evaluate toxicity of the SMT and its intermediates, their developmental toxicity, mutagenicity, bioconcentration factor, and acute toxicity (oral rat) were assessed by quantitative structure-activity relationship prediction using the T.E.S.T. The data of toxicity category was summarized in Table S6 and toxicity analyses were shown in Fig. 10. From Fig. 10a, P3, P2, and P1 in pathway 1, as well as P6 in pathway 3, exhibited higher developmental toxicity values compared to SMT. On the other hand, the P4, P5 in pathway 2 and P7, P8 in pathway 3 demonstrated significantly reduced developmental toxicity values, with P5 even reaching a level of “developmental non-toxicity”. The intermediates of pathway 1 displayed higher mutagenic activity in

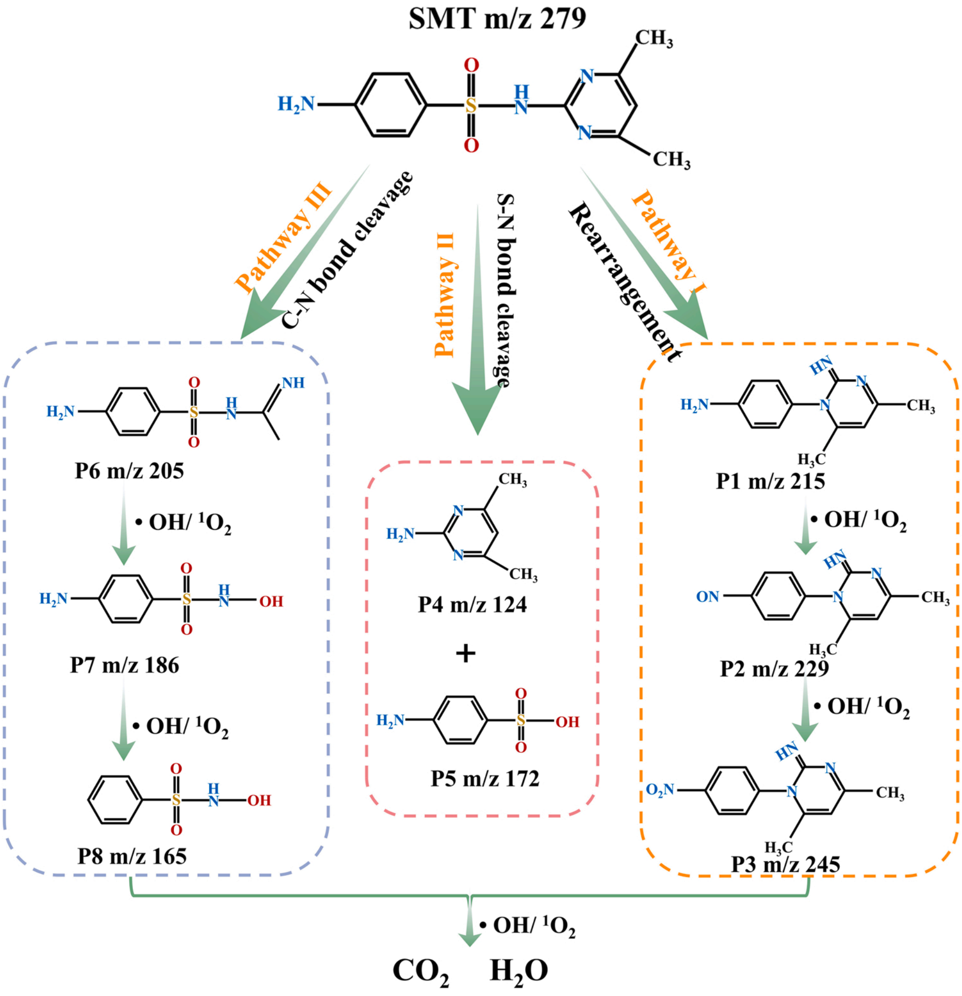

Fig. 9. Proposed degradation pathway of SMT in the HEF system.

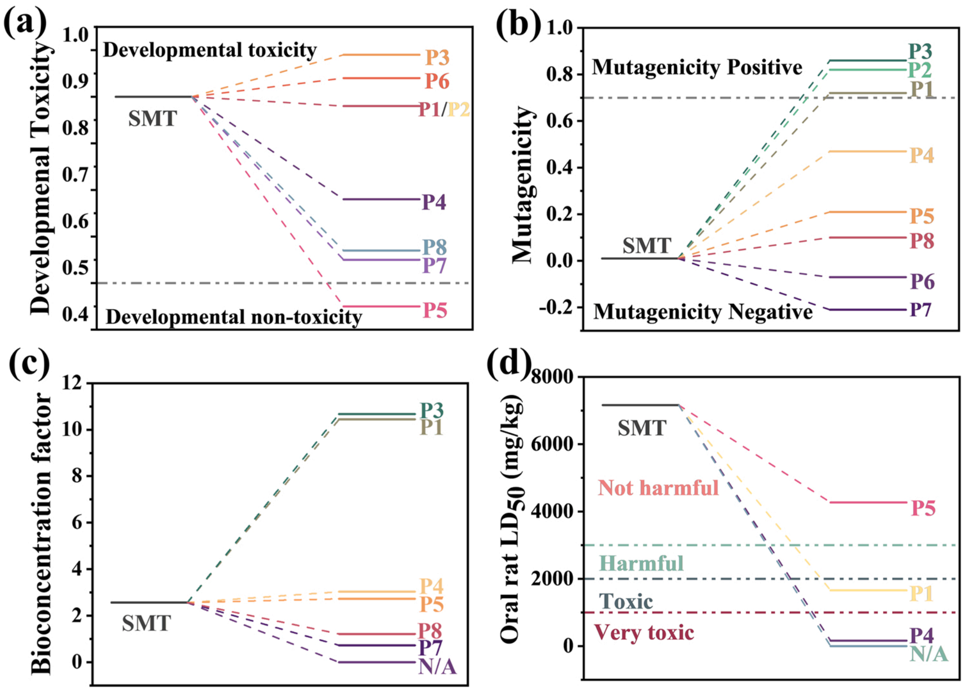

Fig. 10. (a) Developmental toxicity; (b) Mutagenicity; (c) Bioaccumulation factor and (d) Oral rat LD_{50} of SMT and its possible degradation intermediates (N/A indicates not predictable).

comparison to both pathways 2 and 3, with P1, P2, and P3 being identified as “mutagenicity positive”. Only mutagenicity values of P6 and P7 were lower than that of SMT (Fig. 10b). In addition, in pathway 1, the bioconcentration factors of P1 and P3 exhibited a significant increase, while the bioconcentration factors of P5, P7, and P8 were lower than those of SMT. P4 showed bioconcentration factors close to SMT (Fig. 10c). In Fig. 10d, the oral rat LD_{50} of P4 was classified as “very toxic”, whereas P5 was determined to be “not harmful” in pathway 2. Furthermore, P1 was categorized as “toxic” in pathway 1. Based on T.E. S.T. prediction, acute toxicity of the intermediates was significantly reduced by the HEF, while mutagenicity, bioconcentration factor, developmental toxicity of the intermediates in pathway 1 surpassed those of SMT. In addition, these intermediates could reach a harmless level by complete mineralization with prolonged degradation time.

4. Conclusions

A conductive CoNiFe-MOF/LDH was synthesized for degradation of SMT by the HEF process. The electrocatalytic performance of CoNiFe-MOF/LDH was greatly improved by conversion of LDH to MOF. And the introduce of Fe could accelerate the transformation between metals and improve degradation rate. The CoNiFe-MOF/LDH catalyst displayed favorable stability, reusability, and resistance. In addition, the CoNiFe-MOF/LDH had efficient degradation capability towards common sulfonamide antibiotics. The degradation process involved the participation of ·OH, $\cdot O_2^-$, and $^1O_2$. The SMT was degraded by three pathways, the potential hazards of SMT and its products could be effectively reduced. In summary, CoNiFe-MOF/LDH has a favorable degradation effect for sulfonamide antibiotics in the HEF process. Nevertheless, the restricted pH range is limited performance of catalysts in the HEF process. The further research of achieving efficient degradation of other pollutants and expanding the pH range to neutral levels is of great importance for large-scale and real water treatment applications.

CRediT authorship contribution statement

Bing-Qing Wu: Writing - original draft, Investigation, Formal analysis, Data curation, Conceptualization. **Shu-Ting Cheng:** Supervision, Methodology, Investigation, Formal analysis, Data curation. **Xiao-Fang Shen:** Writing - review & editing, Supervision, Resources, Funding acquisition, Conceptualization. **Yue-Hong Pang:** Writing - review & editing, Validation, Supervision, Project administration, Investigation, Funding acquisition, Formal analysis.

Declaration of Competing Interest

The authors declare that they have no known competing financial interests personal relationships that could have appeared to influence the work reported in this paper.

Data availability

Data will be made available on request.

Acknowledgments

This work was supported by the National Natural Science Foundation of China (22276077, 21976070) and the Postgraduate Research & Practice Innovation Program of Jiangsu Province (KYCX23_2515).

Appendix A. Supporting information

Supplementary data associated with this article can be found in the online version at doi:10.1016/j.jece.2024.112426.

References

[1] J. Hu, X. Li, F. Liu, W. Fu, L. Lin, B. Li, Comparison of chemical and biological degradation of sulfonamides: solving the mystery of sulfonamide transformation, J. Hazard. Mater. 424 (2022) 127661, https://doi.org/10.1016/j.jhazmat.2021.127661.

[2] L. Wei, Z. Su, Q. Yue, X. Huang, M. Wei, J. Wang, Microplastics, heavy metals, antibiotics, and antibiotic resistance genes in recirculating aquaculture systems, Trac-Trend Anal. Chem. 172 (2024) 117564, https://doi.org/10.1016/j.trac.2024.117564.

[3] S. Shao, Y. Hu, J. Cheng, Y. Chen, Research progress on distribution, migration, transformation of antibiotics and antibiotic resistance genes (ARGs) in aquatic environment, Crit. Rev. Biotechnol. 38 (2018) 1195–1208, https://doi.org/10.1080/07388551.2018.1471038.

[4] F.C. Cabello, H.P. Godfrey, A. Tomova, L. Ivanova, H. Dölz, A. Millanao, A. H. Buschmann, Antimicrobial use in aquaculture re-examined: its relevance to antimicrobial resistance and to animal and human health, Environ. Microbiol. 15 (2013) 1917–1942, https://doi.org/10.1111/1462-2920.12134.

[5] P. Kovalakova, L. Cizmas, T.J. McDonald, B. Marsalek, M. Feng, V.K. Sharma, Occurrence and toxicity of antibiotics in the aquatic environment: a review, Chemosphere 251 (2020) 126351, https://doi.org/10.1016/j.chemosphere.2020.126351.

[6] S. Yuan, H. Zhang, S. Yuan, Theoretical insights into the uptake of sulfonamides onto phospholipid bilayers: mechanisms, interaction and toxicity evaluation, J. Hazard. Mater. 435 (2022) 129033, https://doi.org/10.1016/j.jhazmat.2022.129033.

[7] S. Huang, J. Yu, C. Li, Q. Zhu, Y. Zhang, E. Lichtfouse, N. Marmier, The effect review of various biological, physical and chemical methods on the removal of antibiotics, Water (Switz.) 14 (2022) 3138, https://doi.org/10.3390/w14193138.

[8] E. Brillas, Progress of homogeneous and heterogeneous electro-Fenton treatments of antibiotics in synthetic and real wastewaters. A critical review on the period 2017–2021, Sci. Total. Environ. 819 (2022) 153102, https://doi.org/10.1016/j.scitotenv.2022.153102.

[9] E. Brillas, Recent development of electrochemical advanced oxidation of herbicides. A review on its application to wastewater treatment and soil remediation, J. Clean. Prod. 290 (2021) 125841, https://doi.org/10.1016/j.jclepro.2021.125841.

[10] Y. Li, B. Yao, Y. Chen, Y. Zhou, X. Duan, Metal-organic frameworks (MOFs) as efficient catalysts for electro-Fenton (EF) reactions: current progress and prospects, Chem. Eng. J. 463 (2023) 142287, https://doi.org/10.1016/j.cej.2023.142287.

[11] Z. Heidari, R. Pelalak, M. Zhou, A critical review on the recent progress in application of electro-Fenton process for decontamination of wastewater at near-neutral pH, Chem. Eng. J. 474 (2023) 145741, https://doi.org/10.1016/j.cej.2023.145741.

[12] Q. Yuan, S. Qu, R. Li, Z.Y. Huo, Y. Gao, Y. Luo, Degradation of antibiotics by electrochemical advanced oxidation processes (EAOPs): performance, mechanisms, and perspectives, Sci. Total. Environ. 856 (2023) 159092, https://doi.org/10.1016/j.scitotenv.2022.159092.

[13] I. Lozano, C.J. Pérez-Guzmán, A. Mora, J. Mahlknecht, C.L. Aguilar, P. Cervantes-Avilés, Pharmaceuticals and personal care products in water streams: occurrence, detection, and removal by electrochemical advanced oxidation processes, Sci. Total. Environ. 827 (2022) 154348, https://doi.org/10.1016/j.scitotenv.2022.154348.

[14] A. Gopinath, L. Pisharody, A. Popat, P.V. Nidheesh, Supported catalysts for heterogeneous electro-Fenton processes: recent trends and future directions, Curr. Opin. Solid. St. M. 26 (2022) 100981, https://doi.org/10.1016/j.cossms.2022.100981.

[15] H. Zhao, Y. Chen, Q. Peng, Q. Wang, G. Zhao, Catalytic activity of MOF(2Fe/Co)/carbon aerogel for improving H_2O_2 and·OH generation in solar photo–electro–Fenton process, Appl. Catal. B. 203 (2017) 127–137, https://doi.org/10.1016/j.apcatb.2016.09.074.

[16] J. Cui, Z. Li, G. Wang, J. Guo, M. Shao, Layered double hydroxides and their derivatives for lithium-sulfur batteries, J. Mater. Chem. A. Mater. 8 (2020) 23738–23755, https://doi.org/10.1039/d0ta08573a.

[17] M. Jana, R. Xu, X.B. Cheng, J.S. Yeon, J.M. Park, J.Q. Huang, Q. Zhang, H.S. Park, Rational design of two-dimensional nanomaterials for lithium-sulfur batteries, Energy Environ. Sci. 13 (2020) 1041–1290, https://doi.org/10.1039/c9ee02049g.

[18] Y. Li, Z. Yan, Z. Sun, Efficient electrocatalytic degradation of sulfamethoxazole with CuAl-LDO/HGF cathode in a neutral heterogeneous electro-Fenton process, J. Environ. Chem. Eng. 11 (2023) 109762, https://doi.org/10.1016/j.jece.2023.109762.

[19] D. Yu, F. Wu, J. He, L. Bai, Y. Zheng, Z. Wang, J. Zhang, Tuned layered double hydroxide-based catalysts inducing singlet oxygen evolution: reactive oxygen species evolution mechanism exploration, norfloxacin degradation and catalysts screen based on machine learning, Appl. Catal. B. 320 (2023) 121880, https://doi.org/10.1016/j.apcatb.2022.121880.

[20] Y. Wang, S. Wang, Z.L. Ma, L.T. Yan, X.B. Zhao, Y.Y. Xue, J.M. Huo, X. Yuan, S. N. Li, Q.G. Zhai, Competitive coordination-oriented monodispersed ruthenium sites in conductive MOF/LDH hetero-nanotree catalysts for efficient overall water splitting in alkaline media, Adv. Mater. 34 (2022) 2107488, https://doi.org/10.1002/adma.202107488.

[21] R. Pelalak, A. Hassani, Z. Heidari, M. Zhou, State-of-the-art recent applications of layered double hydroxides (LDHs) material in Fenton-based oxidation processes for water and wastewater treatment, Chem. Eng. J. 474 (2023) 145511, https://doi.org/10.1016/j.cej.2023.145511.

[22] S. Huang, Y. Wang, S. Qiu, J. Wan, Y. Ma, Z. Yan, Q. Xie, In-situ fabrication from MOFs derived MnxCo$_3$-x@C modified graphite felt cathode for efficient electro-Fenton degradation of ciprofloxacin, Appl. Surf. Sci. 586 (2022) 152804, https://doi.org/10.1016/j.apsusc.2022.152804.

[23] Y. Liu, Y. Wei, M. Liu, Y. Bai, X. Wang, S. Shang, C. Du, W. Gao, J. Chen, Y. Liu, Face-to-face growth of wafer-scale 2D semiconducting MOF films on dielectric substrates, Adv. Mater. 33 (2021) 2007741, https://doi.org/10.1002/adma.202007741.

[24] Y. Wang, L. Yan, K. Dastafkan, C. Zhao, X. Zhao, Y. Xue, J. Huo, S. Li, Q. Zhai, Lattice matching growth of conductive hierarchical porous MOF/LDH heteronanotube arrays for highly efficient water oxidation, Adv. Mater. 33 (2021) 2006351, https://doi.org/10.1002/adma.202006351.

[25] W. Sun, L. Zhou, G. Liu, Y. Zheng, H. Zou, J. Song, Enhanced electro-Fenton degradation of sulfamethazine using Co-based selenite modified graphite cathode via in-situ generation of ·OH, Chem. Eng. J. 463 (2023) 142419, https://doi.org/10.1016/j.cej.2023.142419.

[26] N.M. Mahmoodi, J. Abdi, M. Taghizadeh, A. Taghizadeh, B. Hayati, A.A. Shekarchi, M. Vossoughi, Activated carbon/metal-organic framework nanocomposite: preparation and photocatalytic dye degradation mathematical modeling from wastewater by least squares support vector machine, J. Environ. Manag. 233 (2019) 660–672, https://doi.org/10.1016/j.jenvman.2018.12.026.

[27] S. Yusuf, A. Moheb, M. Dinari, Green phenol hydroxylation by ultrasonic-assisted synthesized Mg/Cu/Al-LDH catalyst with different molar ratios of Cu^{2+}/Mg^{2+}, Res. Chem. Inter. 47 (2021) 1297–1313, https://doi.org/10.1007/s11164-021-04402-0.

[28] Z. Wu, Y. Gu, S. Xin, L. Lu, Z. Huang, M. Li, Y. Cui, R. Fu, S. Wang, CuxNiyCo-LDH nanosheets on graphene oxide: an efficient and stable Fenton-like catalyst for dual-mechanism degradation of tetracycline, Chem. Eng. J. 434 (2022) 134574, https://doi.org/10.1016/j.cej.2022.134574.

[29] F. Wu, J. Nan, T. Wang, Z. Ge, B. Liu, M. Chen, X. Ye, Highly selective electrosynthesis of H_2O_2 by N, O co-doped graphite nanosheets for efficient electro-Fenton degradation of p-nitrophenol, J. Hazard Mater. 446 (2023) 130733, https://doi.org/10.1016/j.jhazmat.2023.130733.

[30] F. Chen, H. Liu, F. Yang, S. Che, N. Chen, C. Xu, N. Wu, Y. Sun, C. Yu, Y. Li, Multifunctional electrocatalyst based on MoCoFe LDH nanoarrays for the coupling of high efficiency electro-Fenton and water splitting process, Chem. Eng. J. 467 (2023) 143274, https://doi.org/10.1016/j.cej.2023.143274.

[31] H. Wang, M. Jing, Y. Wu, W. Chen, Y. Ran, Effective degradation of phenol via Fenton reaction over CuNiFe layered double hydroxides, J. Hazard. Mater. 353 (2018) 53–61, https://doi.org/10.1016/j.jhazmat.2018.03.053.

[32] Y. Wang, L. Li, P. Dai, L. Yan, L. Cao, X. Gu, X. Zhao, Missing-node directed synthesis of hierarchical pores on a zirconium metal-organic framework with tunable porosity and enhanced surface acidity: via a microdroplet flow reaction, J. Mater. Chem. A. 5 (2017) 22372–22379, https://doi.org/10.1039/c7ta06060b.

[33] X. Liu, J. Wei, Y. Wu, J. Zhang, L. Xing, Y. Zhang, G. Pan, J. Li, M. Xu, J. Li, Performances and mechanisms of microbial nitrate removal coupling sediment-based biochar and nanoscale zero-valent iron, Bioresour. Technol. 345 (2022) 126523, https://doi.org/10.1016/j.biortech.2021.126523.

[34] F. Li, X. Ding, Q. Cao, Y. Qin, C. Wang, A ZIF-derived hierarchically porous Fe-Zn-N-C catalyst synthesized: via a two-stage pyrolysis for the highly efficient oxygen reduction reaction in both acidic and alkaline media, Chem. Commun. 55 (2019) 13979–13982, https://doi.org/10.1039/c9cc07489a.

[35] Z. Xue, Y. Li, Y. Zhang, W. Geng, B. Jia, J. Tang, S. Bao, H. Wang, Y. Fan, Z. Wei, Z. Zhang, Z. Ke, G. Li, C. Su, Modulating electronic structure of metal-organic framework for efficient electrocatalytic oxygen evolution, Adv. Energy Mater. 8 (2018) 1801564, https://doi.org/10.1002/aenm.201801564.

[36] L. Liu, Y. Li, Y. Pang, Y. Lan, L. Zhou, Activation of peroxymonosulfate with $CuCo_2O_4$@kaolin for the efficient degradation of phenacetin, J. Environ. Chem. Eng. 11 (2020) 109762, https://doi.org/10.1016/j.cej.2020.126014.

[37] R.H. Monjoghtapeh, A.M. Zardkhoshoui, Hosseiny, S.S. Davarani, Hierarchical $MnCo_2S_4$ nanowires/NiFe LDH nanosheets/graphene: a promising binder-free positive electrode for high-performance supercapacitors, Electrochim. Acta 338 (2020) 135891, https://doi.org/10.1016/j.electacta.2020.135891.

[38] X. Du, W. Fu, P. Su, Q. Zhang, M. Zhou, FeMo@porous carbon derived from MIL-53 (Fe)@MoO_3 as excellent heterogeneous electro-Fenton catalyst: co-catalysis of Mo, J. Environ. Sci. 127 (2023) 652–666, https://doi.org/10.1016/j.jes.2022.06.031.

[39] M. Guo, M. Lu, H. Zhao, F. Lin, F. He, J. Zhang, S. Wang, P. Dong, C. Zhao, Efficient electro-Fenton catalysis by self-supported CFP@$CoFe_2O_4$ electrode, J. Hazard. Mater. 423 (2022) 127033, https://doi.org/10.1016/j.jhazmat.2021.127033.

[40] H. Wang, Y. Wang, J. Zhang, X. Liu, S. Tao, Electronic structure engineering through Fe-doping CoP enables hydrogen evolution coupled with electro-Fenton, Nano. Energy 84 (2021) 105943, https://doi.org/10.1016/j.nanoen.2021.105943.

[41] X. Zhao, B. Pattengale, D. Fan, Z. Zou, Y. Zhao, J. Du, J. Huang, C. Xu, Mixed-node metal-organic frameworks as efficient electrocatalysts for oxygen evolution reaction, ACS Energy Lett. 3 (2018) 2520–2526, https://doi.org/10.1021/acsenergylett.8b01540.

[42] H. Wang, C. Tang, L. Wang, Z. Sun, X. Hu, MOF-derived Co/Fe@NPC-500 with large amounts of low-valent metals as an electro-Fenton cathode for efficient degradation of ceftazidime, Appl. Catal. B. 333 (2023) 122755, https://doi.org/10.1016/j.apcatb.2023.122755.

[43] H. Qi, X. Shi, Z. Liu, Z. Yan, Z. Sun, In situ etched graphite felt modified with $CuFe_2O_4$/Cu_2O/Cu catalyst derived from CuFe PBA for the efficient removal of sulfamethoxazole through a heterogeneous electro-Fenton process, Appl. Catal. B. 331 (2023) 122722, https://doi.org/10.1016/j.apcatb.2023.122722.

[44] R. Dong, P. Han, H. Arora, M. Ballabio, M. Karakus, Z. Zhang, C. Shekhar, P. Adler, P.S. Petkov, A. Erbe, S.C.B. Mannsfeld, C. Felser, T. Heine, M. Bonn, X. Feng, E. Cánovas, High-mobility band-like charge transport in a semiconducting two-dimensional metal–organic framework, Nat. Mater. 17 (2018) 1027–1032, https://doi.org/10.1038/s41563-018-0189-z.

[45] M. Xu, J. Wei, X. Cui, J. Li, G. Pan, Y. Li, Z. Jiang, X. Niu, N. Cui, J. Li, High-efficiency electro-Fenton process based on in-situ grown CoFeCe-LDH@CFs free-standing cathodes: correlation of cerium and oxygen vacancies with H_2O_2, Chem. Eng. J. 455 (2023) 140922, https://doi.org/10.1016/j.cej.2022.140922.

[46] C. Zhang, M. Zhou, G. Ren, X. Yu, L. Ma, J. Yang, F. Yu, Heterogeneous electro-Fenton using modified iron-carbon as catalyst for 2,4-dichlorophenol degradation:

influence factors, mechanism and degradation pathway, Water Res. 70 (2015) 414–424, https://doi.org/10.1016/j.watres.2014.12.022.

[47] Y. Jin, P. Huang, X. Chen, L. Li, C. Lin, X. Chen, R. Ding, J. Liu, R. Chen, Ciprofloxacin degradation performances and mechanisms by the heterogeneous electro-Fenton with flocculated fermentation biochar, Environ. Pollut. 324 (2023) 121425, https://doi.org/10.1016/j.envpol.2023.121425.

[48] X. Du, W. Fu, P. Su, J. Cai, M. Zhou, Internal-micro-electrolysis-enhanced heterogeneous electro-Fenton process catalyzed by Fe/Fe_3C@PC core–shell hybrid for sulfamethazine degradation, Chem. Eng. J. 398 (2020) 125681, https://doi.org/10.1016/j.cej.2020.125681.

[49] X. Du, W. Fu, P. Su, Q. Zhang, M. Zhou, S-doped MIL-53 as efficient heterogeneous electro-Fenton catalyst for degradation of sulfamethazine at circumneutral pH, J. Hazard. Mater. 424 (2022) 127674, https://doi.org/10.1016/j.jhazmat.2021.127674.

[50] M. Priyadarshini, A. Ahmad, M.M. Ghangrekar, Efficient upcycling of iron scrap and waste polyethylene terephthalate plastic into Fe_3O_4@C incorporated MIL-53 (Fe) as a novel electro-Fenton catalyst for the degradation of salicylic acid, Environ. Pollut. 322 (2023) 121242, https://doi.org/10.1016/j.envpol.2023.121242.

[51] T. Xu, X. Zheng, Y. Zhou, C. Zhu, B. Hu, X. Lei, X. Zhang, G. Yu, Study on the treatment of Cu^{2+}-organic compound wastewater by electro-Fenton coupled pulsed AC coagulation, Chemosphere 280 (2021) 130679, https://doi.org/10.1016/j.chemosphere.2021.130679.

[52] W. Zhou, L. Xie, J. Gao, R. Nazari, H. Zhao, X. Meng, F. Sun, G. Zhao, J. Ma, Selective H_2O_2 electrosynthesis by O-doped and transition-metal-O-doped carbon cathodes via O_2 electroreduction: a critical review, Chem. Eng. J. 410 (2021) 128368, https://doi.org/10.1016/j.cej.2020.128368.

[53] G. Dong, B. Chen, B. Liu, L.J. Hounjet, Y. Cao, S.R. Stoyanov, M. Yang, B. Zhang, Advanced oxidation processes in microreactors for water and wastewater treatment: development, challenges, and opportunities, Water Res. 211 (2022) 118047, https://doi.org/10.1016/j.watres.2022.118047.

[54] Y. Chu, C. Liu, R. Wang, H. Chen, Development of heterogenous electro-Fenton process with immobilized $FeWO_4$ catalyst for the degradation of tetracycline and the treatment of crude oil tank cleaning wastewater in neutral medium, Chem. Eng. J. 465 (2023) 142964, https://doi.org/10.1016/j.cej.2023.142964.

[55] Q. Yi, J. Ji, B. Shen, C. Dong, J. Liu, J. Zhang, M. Xing, Singlet oxygen triggered by superoxide radicals in a molybdenum cocatalytic Fenton reaction with enhanced REDOX activity in the environment, Environ. Sci. Technol. 53 (16) (2019) 9725–9733, https://doi.org/10.1021/acs.est.9b01676.

[56] P. Su, W. Fu, X. Du, J. Guo, M. Zhou, Cost-effective degradation of pollutants by in-situ electrocatalytic process on Fe@BN-C bifunctional cathode: Formation of $^1O_2$ with high selectivity under nanoconfinement, Chem. Eng. J. 452 (2023) 139693, https://doi.org/10.1016/j.cej.2022.139693.

[57] P. Su, W. Fu, X. Du, G. Song, M. Zhou, Confined Fe^0@CNTs for highly efficient and super stable activation of persulfate in wide pH ranges: radicals and non-radical co-catalytic mechanism, Chem. Eng. J. 420 (2021) 129446, https://doi.org/10.1016/j.cej.2021.129446.